MINISTRY OF NATIONAL DEFENSE
MILITARY TECHNICAL ACADEMY

NGUYEN THANH

NONLINEAR DISTORTIONS AND COUNTERMEASURES FOR PERFORMANCE IMPROVEMENTS IN CONTEMPORARY RADIO COMMUNICATION SYSTEMS

SUMMARY OF TECHNICAL DOCTORAL THESIS

Ha Noi - 2019

LIST OF PUBLICATIONS

1. **Nguyen Thanh**, Nguyen Tat Nam, and Nguyen Quoc Binh, "Automatic phase compensation in MIMO-STBC systems with nonlinear distortion incurred by high power amplifiers," *in Proceedings of the 2017 Advanced Technology for Communications Conference - ATC 2017*, Quy Nhon, Viet Nam, pp. 86-91, Oct. 18-20, 2017.

2. **Nguyen Thanh**, Nguyen Tat Nam, and Nguyen Quoc Binh, "Performance of a phase estimation method under different nonlinearities incurred by high power amplifiers in MIMO-STBC systems," *in Proceedings of the Conference on Information and Computer Science - NICS 2017*, Ha Noi, Viet Nam, pp. 42-47, Nov. 24-25, 2017.

3. **Nguyễn Thành**, Nguyễn Tất Nam, Nguyễn Quốc Bình, "Ảnh hưởng của méo phi tuyến do bộ KĐCS đến hệ thống MIMO-STBC trong trường hợp có sử dụng bộ méo trước và bộ lọc tạo dạng tín hiệu," *Tạp chí Khoa học và Kỹ thuật, Học viện Kỹ thuật Quân sự*, trang 74-88, số 188, tháng 2 năm 2018.

4. **Nguyen Thanh**, Nguyen Quoc Binh, Nguyen Thi Phuong Hoa, "Phase estimation and compensation under different nonlinearities incurred by high power amplifiers in MIMO-STBC systems," *Journal of Science and Technique - Military Technical Academy*, pp. 59-74, No. 191, Jun. 2018.

5. **Nguyen Thanh**, Nguyen Tat Nam, Nguyen Quoc Binh, "On the reasonableness of nonlinear models for high power amplifiers and their applications in communication system simulations," *Journal of Military Science and Technology - Academy of Military Science and Technology*, pp. 86-99, No. 55, Jun. 2018.

Summary of major findings and contributions

Major contributions of the thesis are as follows.

1. Evaluating nonlinear HPA models regarding to problem of simulating intermodulation products (IMP). Proposing the polysine model for precise simulation of IMPs, especially for signals with complex structures.
2. Proposing the use of predistortion schemes for MIMO-STBC systems based on thorough analyses of the nonlinear HPA effects on these systems with transmit/receive filters introduced in the model.
3. Proposing an automatic, efficient phase estimation and compensation diagram for MIMO-STBC systems using M-QAM signaling incurred with nonlinear distortions from different HPA types of both TWTAs and SSPAs.

Suggested extensions

1. The simulation results have initially confirmed the advantages of the proposed polysine model as well as the pre-compensation and pos-compensation schemes for nonlinear distortions, the hardware experimental tests will solidify the achieved results and confirm the practical applicability of these proposals;
2. Researches on the effects of nonlinear distortions for updated MIMO technologies and systems such as spatial modulation, multi-user MIMO, etc. are still very limited;
3. Another research direction that has not been widely discussed for MIMO-STBC systems is the evaluation of system performance degradation under the simultaneous effects of nonlinear distortions and other effects such as linear distortions, or hardware impairments like local oscillator phase noise, sampling jitter, sampling frequency offset, carrier frequency offset, IQ imbalance, RF coupling, cross-talk,...
4. The M-APSK modulation schemes are preferred in the new satellite communication standards since they have many advantages over M-QAM schemes. However, nonlinear distortions with the phase rotation effect are always present. The ability to apply a phase estimation and compensation solution for these M-APSK schemes is still left open.

INTRODUCTION

1. Background of research:

A practical high power amplifier (HPA) does have a nonlinear input-output characteristic, thus, distorting the output signal [45, 55]. Hence, modeling and analyzing nonlinear HPA transfer functions, and specifically, investigating effects of these characteristics to modern digital communication systems are still contemporary topics widely studied. Thoughtful understanding the causes of errors in simulating intermodulation products for conventional models such as Saleh, Rapp, polynomial,... and overcoming these defects by constructing a suitable HPA model are then really strong but challenging research motivations.

For SISO systems, [1, 4, 11, 13] resolved several nonlinear HPA-related problems such as evaluating separate/concurrent effects of nonlinear/linear distortions, applying optimum additional phase shifting solution. Recently, [3] extended these results to MIMO-STBC systems accenting on satellite communications. However, there are several topics which are not rigorously discussed and also are not extended to new directions. Therefore, this work entitled "Nonlinear distortions and countermeasures for performance improvements in contemporary radio communication systems", focuses on dealing to such problems.

2. Major findings and contributions:

1. Evaluating nonlinear HPA models regarding to problem of simulating intermodulation products (IMP). Proposing the polysine model for precise simulation of IMPs, especially for signals with complex structures.
2. Proposing the use of predistortion schemes for MIMO-STBC systems based on thorough analyses of the nonlinear HPA effects on these systems with transmit/receive filters introduced in the model.
3. Approximating nonlinear phase distortion by a linear model. Based on that, proposing an automatic, efficient phase estimation and compensation diagram for MIMO-STBC systems using M-QAM signaling.

3. Thesis outline:

This thesis includes about 120 pages and is organized in four chapters except for the foreword, conclusion and references.

Chapter 1

Introduction to Nonlinear Distortion and Practical MIMO-STBC Systems

1.1 Main causes of nonlinear distortions in radio communication systems

In practice, radio transmitters often have structure consisting of several typical stages such as baseband signal processing, digital-to-analog conversion, modulation, frequency up-conversion, filtering, amplifications, antenna,... Among these parts, radio frequency HPA is one of the most power-consuming components and is the main cause of nonlinear distortions [9, 22, 23, 55].

1.2 Nonlinear HPA model classification

Figure 1.1 describes the HPA model classification with related features. Here, models marked by gray will be studied in detail throughout the thesis. Let's $r(t)$ and $\phi(t)$ are the amplitude modulation (AM) and phase modulation (PM) of the input $x(t) = r(t)e^{j\phi(t)}$. The input-output nonlinear relation $F(.)$ could be represented by AM-AM and AM-PM functions $F_a(r)$, $F_p(r)$ as

$$y(t) = F(x(t)) = F_a(r(t))e^{j(\phi + F_p(r(t)))}. \tag{1.1}$$

- *Ideal model* is the perfectly linearized model for HPA with

$$y = gx, \text{ or equivalently, } F_a(r) = gr, F_p(r) = 0, \tag{1.2}$$

where, $x = x(t)$, $y = y(t)$, and $g > 0$ is the (real-valued) linear gain.

- *Linearized model* is the simplest HPA model without considering output magnitude clipping for nonlinear characteristic

$$y = gx + n, \tag{1.3}$$

where, g has the same meaning as in (1.2), n is an uncorrelated nonlinear distortion approximated by a Gaussian noise [16, 69].

- *Soft limiter* is the simplest HPA model considering output clipping [52].

$$F_a(r) = \begin{cases} r, & |r| < A_{\text{is}} \\ A_{\text{is}}, |r| \geqslant A_{\text{is}}, \end{cases} \tag{1.4}$$

$$F_p(r) = 0, \tag{1.5}$$

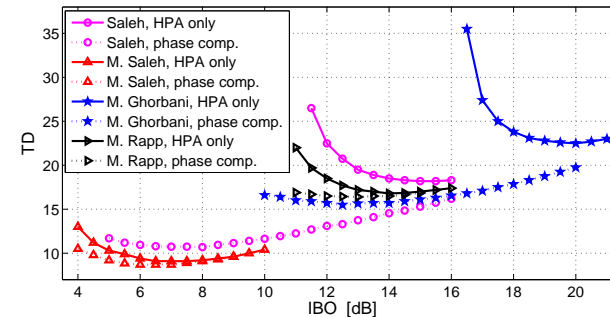conversions such as for Saleh or modified Ghorbani models.

Figure 4.5: $TD(IBO)$ with/without phase compensation at $BER = 10^{-3}$.

4.4.4 Bit error ratio

From Figure 4.6, the savings of E_b/N_0 for phase-compensated systems with nonlinearities having small phase conversions are still significant (more than 2 dB for modified Saleh model and more than 3 dB for modified Rapp model at $BER = 10^{-3}$). The gains for phase-compensated systems with strong phase conversions (with Saleh, or modified Ghorbani models) are really huge.
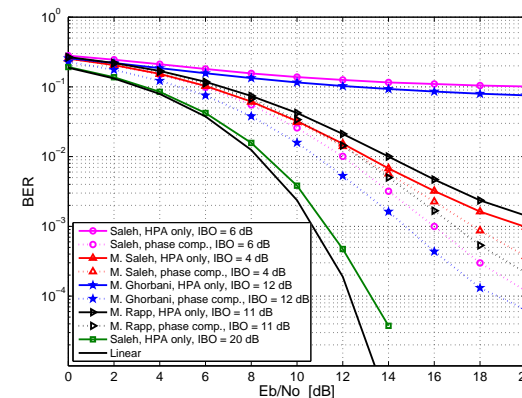

Figure 4.6: $BER(E_b/N_0)$ with/without phase compensation.

4.5 Summary of chapter 4

In this chapter, the effects of nonlinear phase distortion incurred by HPAs on the MIMO-STBC system are analyzed in detail. Based on that, a phase estimation algorithm and phase compensation scheme are proposed. The effectiveness of proposed scheme is examined using a series of typical HPA models.

Table 4.1: Estimated phases and their variances for different nonlinearities.

Saleh				M. Saleh				M. Ghorbani				M. Rapp			
IBO [dB]	ϕ_{33} [deg]	$\hat{\phi}_0$ [deg]	var($\hat{\phi}_0$) [deg]^2	IBO [dB]	ϕ_{33} [deg]	$\hat{\phi}_0$ [deg]	var($\hat{\phi}_0$) [deg]^2	IBO [dB]	ϕ_{33} [deg]	$\hat{\phi}_0$ [deg]	var($\hat{\phi}_0$) [deg]^2	IBO [dB]	ϕ_{33} [deg]	$\hat{\phi}_0$ [deg]	var($\hat{\phi}_0$) [deg]^2
6	19.7	17.5	0.085	4	-4.3	-3.1	0.137	9	21.2	18.6	0.334	10	-8.2	-5.4	0.183
7	18.6	16.3	0.025	5	-3.8	-2.7	0.042	10	20.5	19.7	0.198	11	-6.4	-4.3	0.121
8	17.5	15.2	0.019	6	-3.3	-2.3	0.019	11	19.6	17.1	0.085	12	-4.7	-3.3	0.042
9	16.2	13.9	0.015	7	-2.8	-1.8	0.008	12	18.6	16.1	0.032	13	-3.3	-2.4	0.031
10	14.8	12.6	0.008	8	-2.1	-1.2	0.008	13	17.5	15.0	0.025	14	-2.2	-1.7	0.020
11	13.4	11.2	0.007	9	-1.5	-0.7	0.007	14	16.2	13.9	0.019	15	-1.5	-1.1	0.010

4.4.2 Optimum proximity of the estimated phases

The phase compensation optimity is depicted in Figure 4.4, where each curve is noted with a solid square marker corresponding to the compensation using estimated phase. Though being incurred by different nonlinearities depending on the HPA models, the optimal compensating phases always approximate to ϕ_{33} as analysed. In general, the proposed phase compensations are suboptimal but performance gains in terms of BER improvements are promising, especially for cases with larger phase rotations (for Saleh or modified Ghorbani models).
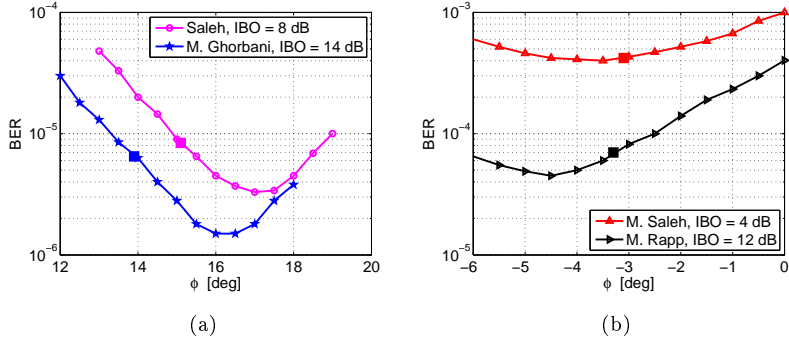

(a)   (b)

Figure 4.4: BER versus compensated phase angle: a) Saleh and modified Ghorbani models; b) Modified Saleh and modified Rapp models.

4.4.3 Total degradation

As clearly seen from Figure 4.5, huge TD gains could be achieved when applying the phase compensations especially for nonlinearities with strong phase

where, A_{is} is the input saturation level (voltage) which in this case with unity gain $g = 1$, is also the output saturation level, $A_{\text{os}} = A_{\text{is}}$.
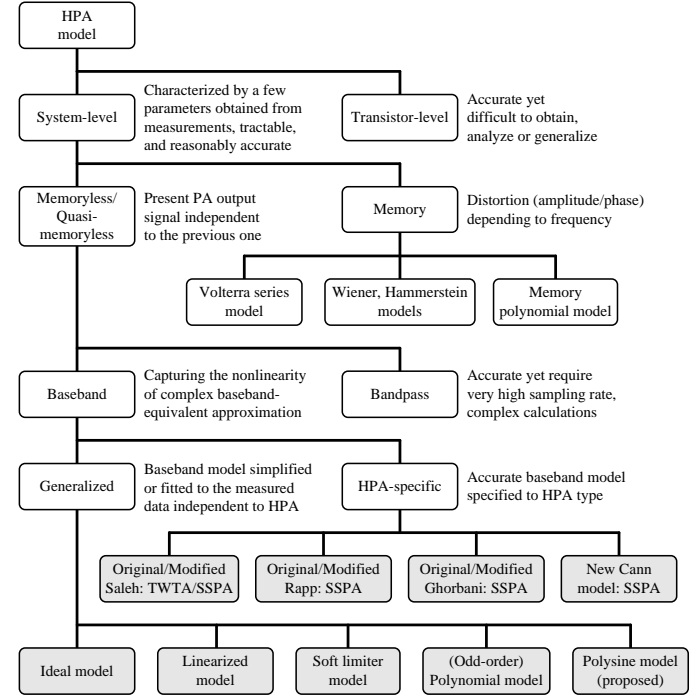

Figure 1.1: HPA modeling classification.

Figure 1.2 illustrates the AM-AM and AM-PM for typical input/output powers, $P_{\text{out}} = F_a(P_{\text{in}})$, and phase shift $\Delta\Phi_{\text{out}} = F_p(P_{\text{in}})$. The quantities represented here will be widely used in quantitative analyses in later chapters.

1.3 Nonlinear HPA distortion effects in SISO systems

In fact, for single-carrier SISO systems, under the influence of HPA nonlinear characteristics, several complex-interrelated effects will be generated with non-constant envelope input signals. However, for simplification in analyses, it can be isolated into separate effects as follows [2]: (a) Creating spectrum regrowth and nonlinear noise; (b) Warping constellation; and (c) Creating nonlinear ISI.

1.4 Multiple-input multiple-output systems

The concept of multiple-input multiple-output began to appear in the mid-1950s in circuit and signal filtering theories for describing diagrams with multiple-input/-output ports [26]. However, in the 1990s, this concept was put on a new
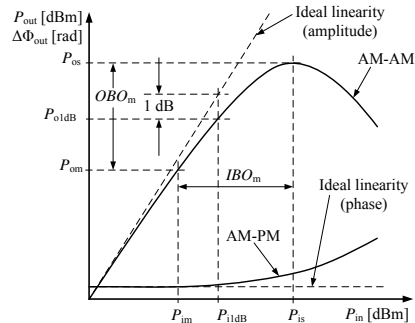
Figure 1.2: Typical amplitude and phase characteristics of an HPA.

look, for a completely different signal processing technique [25], using to index signals from different transmit/receive antennas "entering/exiting" into/from the radio medium. Then, three new multi-antenna techniques have been developed: *spatial diversity* (SD), *spatial multiplexing* (SM), and *smart antenna* (SA).

1.5 MIMO in satellite communication systems

The satellite-to-ground great distances make the radio links actually become *keyhole* channels, causing significant performance reduction [93]. Therefore, researches relating to MIMO satellite communications (SatCom) are currently focused on land mobile satellite (LMSat) systems exploiting the following diversity configurations: (a) Site; (b) Satellite; and (c) Polarization diversity.
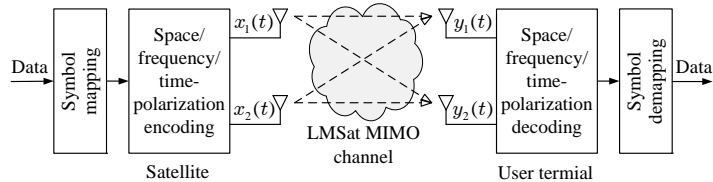

Figure 1.3: Dual-polarized MIMO LMSat system model.

Moreover, the general trend of MIMO LMSat studies accents to the use of polarization diversity [8,20,36,49,59] due to recent advances in antenna design. Analyzing the dual-polarization MIMO LMSat system performance has thoroughly been studied in [20,36,48,49,75], but most do not mention the practical nonlinear HPAs, or introduce them into the system model for simulation but do not perform any quantitative analyses or assessments. Next, effects of nonlinear HPAs to MIMO LMSat system shown in Figure 1.3 is analyzed briefly to get an overview of the arising problems that will be dealt with in this thesis.

4.3.3 Harmonic approximation

Here, only the 4-th order harmonic in (4.6) is considered $(N = 1)$,

$$X_1 = 4A_4(r)\sin(4\phi), \quad X_2 = -16A_4(r)\cos(4\phi). \qquad (4.10)$$

Then $A_4(r)$ could be solved using the Lagrange multiplier method [79]

$$A_4(r) = -\lambda D_4(r)/(2N_4(r)), \qquad (4.11)$$

where, λ is a Lagrange multiplier, having no effect to the estimation result, and

$$N_4(r) = 16 \int_0^{2\pi} \sin^2(4\phi)p(r,\phi)d\phi, \qquad (4.12)$$

$$D_4(r) = -16 \int_0^{2\pi} \cos(4\phi)p(r,\phi)d\phi. \qquad (4.13)$$

4.3.4 Biharmonic approximation

Here, both the 4-th and 8-th order harmonics are used $(N = 2)$,

$$X_1 = 4A_4(r)\sin(4\phi) + 8A_8(r)\sin(8\phi), \qquad (4.14)$$

$$X_2 = -16A_4(r)\cos(4\phi) - 64A_8(r)\cos(8\phi). \qquad (4.15)$$

4.4 Performance evaluation of the phase estimation and phase compensation scheme

System parameters are as generating Figure 4.3(a). Signals are transmitted in frames of size $2K = 2000$ symbols, and multiframe of size 100 frames. Their phases are then estimated by (4.8) using biharmonic approximation.

4.4.1 Performance of the phase estimator

The estimation quality, in terms of estimation variance, $\mathrm{var}(\widehat{\phi}_0)$, is reliable. With frame and multiframe sizes as set, for all cases, the standard deviation is always smaller than 0.6°, which is a relatively small value for the phase estimation problem, even for terrestrial digital microwave or satellite applications [22, 61]. Moreover, in small phase rotation cases (modified Saleh or modified Rapp models at larger IBOs), the standard deviation is always about one tenth of the estimated value. Therefore, it is not necessary to increase the frame and multiframe sizes to improve the estimation reliability.

4.3.2 Optimal blind feedforward phase estimation

The maximum likelihood (ML) estimation of rotated phase ϕ_0 in (4.1) is determined by maximizing, regarding to ϕ_0 the log-likelihood function (LLF)

$$\hat{\phi}_0 = \arg\max_{\phi_0} LLF(\phi_0|\{y_k\}), \qquad (4.2)$$

here, $LLF(.)$ is given by

$$LLF(\phi_0|\{y_k\}) = \sum_{k=1}^{2K} F_\phi(\phi_0|y_k), \qquad (4.3)$$

where, $F_\phi(\phi_0|y)$ is the probability density function of sample $y = re^{j\phi}$

$$F_\phi(\phi_0|y) = \log\left(\frac{1}{2\pi\sigma^2 M^2}\sum_{\substack{m=1,\\n=1}}^{M} e^{\left(-\frac{|re^{j(\phi-\phi_0)}-s_m-s_n|^2}{2\sigma^2}\right)}\right). \qquad (4.4)$$

It is possible to recast (4.4) in the form of circular harmonic expansion [50] as

$$LLF(\phi_0|re^{j\phi}) = \frac{A_0(r)}{2} + \sum_{n=1}^{\infty} A_n(r)\cos(n\phi - n\phi_0 + \theta_n(r)). \qquad (4.5)$$

After truncating (4.5), the target function is of the form

$$\hat{\phi}_0 = \arg\max_{\phi_0}\mathrm{Re}\left(\sum_{n=1}^{N} F_{4n}(\{y_k\})e^{-j4n\phi_0}\right)$$
$$= \arg\max_{\phi_0} f(\phi_0), \qquad (4.6)$$

By approximating the target function $f(\phi_0)$ in (4.6) to the second order Taylor series in the vicinity of ϕ_0, assumed to be zero,

$$f(\phi_0) \approx f(0) + \phi_0 f'(0) + \phi_0^2 f''(0)/2 \to \max_{\phi_0}, \qquad (4.7)$$

then, the maximum of this approximation is simply determined as

$$\hat{\phi}_0 = -f'(0)/f''(0), \qquad (4.8)$$

where, the first and second derivatives of the target function $f(\phi_0)$ are given by

$$f'(0) = \sum_{k=1}^{2K} X_{1k}, \quad f''(0) = \sum_{k=1}^{2K} X_{2k}. \qquad (4.9)$$

1.6 Nonlinear HPA distortion effects in MIMO systems

In addition to incurring similar effects as for conventional SISO systems, additional detrimental effects arise in nonlinear MIMO systems. Consider the MIMO-STBC Alamouti coding [7] with nonlinear HPAs as in Figure 1.4.
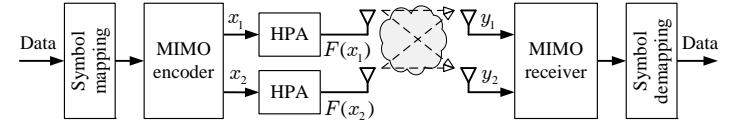

Figure 1.4: Simplified MIMO system with nonlinear HPA.

The MIMO encoder outputs the encoding matrix $\mathbf{X}$ in the form of

$$\mathbf{X} = \begin{bmatrix} \mathbf{x}_1 \\ \mathbf{x}_2 \end{bmatrix} = \begin{bmatrix} x_{1,k} & x_{1,k+1} \\ x_{2,k} & x_{2,k+1} \end{bmatrix} = \begin{bmatrix} s_k & -s_{k+1}^* \\ s_{k+1} & s_k^* \end{bmatrix}, \qquad (1.6)$$

Alamouti coding is an orthogonal design, namely

$$\mathbf{x}_1\mathbf{x}_2^H = [s_k \quad -s_{k+1}^*]\begin{bmatrix} s_{k+1}^* \\ s_k \end{bmatrix} = 0, \qquad (1.7)$$

This orthogonality will be broken if passing signals through nonlinear HPAs

$$\mathbf{x}_1\mathbf{x}_2^H = [F(s_k) \quad F(-s_{k+1}^*)]\begin{bmatrix} F(s_{k+1}^*) \\ F(s_k) \end{bmatrix} \neq 0. \qquad (1.8)$$

Thus, the transmit diversity gain is deteriorated under the appearance of non-orthogonal components due to nonlinear distortions. The problem will become even more complicated when further considering the transmit/receive filters. The nonlinear ISI, generated from each individual transmit branch continues to affect orthogonality in a manner similar to what useful signals influence shown above, or the nonlinear inter-antenna interference (non-orthogonality components) continues to deteriorate receive signals in each antenna branch under the memory effect of the receive matched filter. Thus, the system performance is poly-degraded in an involved manner.

1.7 Summary of chapter 1

The background knowledge directly related to the research objects including the nonlinear HPA model, MIMO techniques with specific implementations to the LMSat systems, and the effects of nonlinear HPAs in MIMO communication systems has been discussed in this chapter. These analyses have clearly shown urgent issues and updated research directions that the thesis can pursue.

Chapter 2

Nonlinear HPA Modeling and Proposed Polysine Model

2.1 Introduction

Primitively, in 1980, Cann [17] introduced an instantaneous nonlinear model for HPAs with variable knee sharpness, relatively convenient for analytical analysis and simulation. However, it must be 16 years later, Litva [62] discovered that this model produces erroneous results for IMPs in the two-tone test. Other studies further showed that this problem does occur particularly for the two-tone testing signal and does not occur with other practically-used signals. The following sections in this chapter will in turn proceed detailed analyses of arising problems and corresponding solutions for the HPA modeling complication.

2.2 Instantaneous nonlinear models

The original Cann instantaneous nonlinear model is given by [17]

$$y = \frac{A_{os} \cdot \text{sgn}(x)}{\left[1 + \left(\frac{A_{os}}{g|x|}\right)^s\right]^{1/s}} = \frac{gx}{\left[1 + \left(\frac{g|x|}{A_{os}}\right)^s\right]^{1/s}}, \tag{2.1}$$

where, sgn(.) is the sign operator; g is the small-signal (linear) gain; A_{os} is the output saturation level; and s is the curve sharpness parameter. Four years after the finding of Litva in 1996 [62], Loyka [65] discovered that the reason is the use of modulus (|.|) function in (2.1), some of whose derivatives at zero do not exist, are undefined, or are infinite. In other words, the function is non-analytic, despite the deceptively smooth appearance of the plotted curves.

Cann then suggested an improved nonlinear instantaneous model as [18]

$$y = \frac{A_{os}}{s} \ln \frac{1 + e^{s(gx/A_{os}+1)}}{1 + e^{s(gx/A_{os}-1)}} - A_{os}, \tag{2.2}$$

The derivatives of new model (2.2) exist and well behave, even with fractional s. Then, it eliminates the shortcomings of previous one (2.1). This is the analyticity and symmetry of this transfer function to resolve the problem.
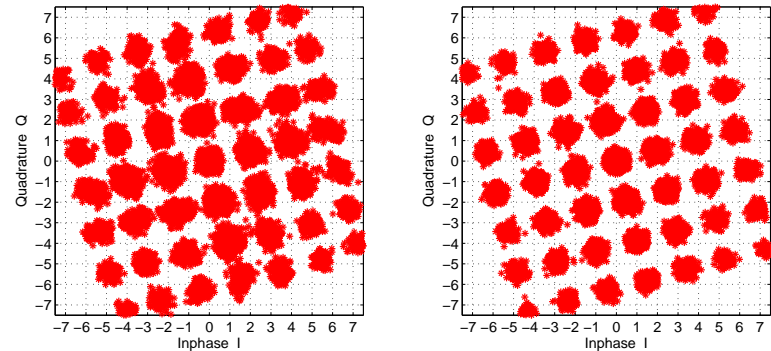
(a)   (b)

Figure 4.3: Receive signal constellations after matched filtering: a) Fully characterized (3.4, 3.5); b) Approximated (4.1).

Gaussian-equivalent noise. This model will be discussed in more detail in the following section with graphical illustration depicted in Figure 4.3(b).

4.3 Phase estimation problem

4.3.1 Gaussian approximation for the nonlinear model

In this work, fading channel effects is temporarily ignored and will be considered in future studies; then the channel coefficients could all be set to unity. Further, by the analysis discussed in previous section, it is reasonable to approximate the signal in time slot k and $k+1$ as

$$\begin{aligned} y_k &= (\bar{s}_k + \bar{s}_{k+1})e^{j\phi_0} + n_k^{equ}, \\ y_{k+1} &= (\bar{s}_k^* - \bar{s}_{k+1}^*)e^{j\phi_0} + n_{k+1}^{equ}, \end{aligned} \tag{4.1}$$

Noting that approximation (4.1) insists on the phase rotation while neglecting the amplitude compression of nonlinear effects. Figure 4.3(b) illustrates this approximation with phase rotation $\phi_0 = 16.2°$, which is the phase conversion of signal point $(3,3)$ in the 16-QAM constellation under the same nonlinearity generating Figure 4.3(a). Regardless of the almost indistinguishable amplitude compression (for large magnitude combined signals) in sub-figure 4.3(a), then there is a close similarity of models (3.4), (3.5) and (4.1). This underlines for the efficient estimation of phase rotation caused by HPA's discussed next.

are focused in: Saleh model (2.3), (2.4); modified Saleh model (2.9), (2.10); modified Ghorbani model (2.11), (2.12); modified Rapp model (2.5), (2.13).
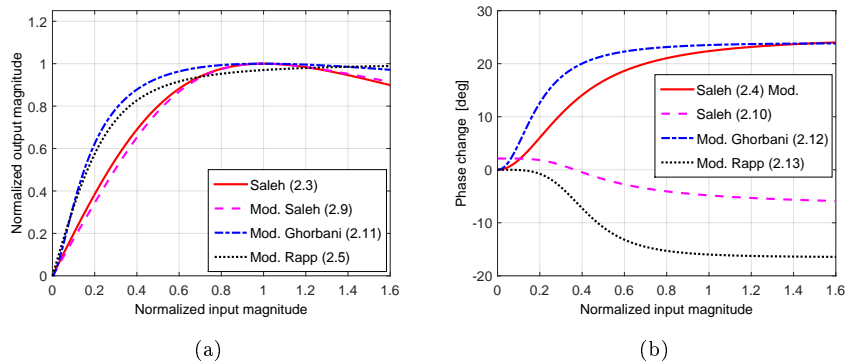

(a)   (b)

Figure 4.2: AM-AM (a) and AM-PM (b) characteristics of considered HPAs.

Figure 4.2 illustrates the amplitude and phase characteristics of all four models above with normalized input and output magnitudes to their corresponding saturation levels for nonlinearity comparison purpose. Obviously, these characteristics are quite different in terms of amplitude and especially of phase distortions. These nonlinearity dissimilarities could affect signal passed through in very different extents and amounts; then, is the proposed phase estimator affected. Details are further discussed in the following sections.

4.2.2 Phase rotation effect incurred by nonlinear HPAs

Receive signals after matched filtering, as fully described by (3.4) and (3.5), are illustrated in Figure 4.3(a), resulted from simulation by parameters: 16-QAM; SRRC filters with roll-off factor $\alpha = 0.2$, input sampling rate $F_d = 1$, output sampling rate $F_s = 16F_d$, group delay $Dl = 10$; HPA follows modified Ghorbani model (2.11) and (2.12) with characteristics plotted in Figure 4.2, $IBO = 14$ dB; $E_b/N_0 = 20$ dB, automatic gain control used at receiving part.

It is further observed that, under the HPA's phase conversion effects, receive signal clusters tend to be almost rotated by the same angle, approximating to the phase conversion for the largest magnitude component signal. The reason is that for every combined signal $y_{l,k}$ by (3.4) and (3.5), there are always components with largest magnitudes, the main factor causing phase rotation for $y_{l,k}$. Therefore, it is reasonable to have good approximation of this nonlinear system to the linear one affected by a fixed phase rotation and an additive

2.3 Envelope nonlinear models

2.3.1 Saleh model

In 1981, Saleh introduced a closed-form TWTA model [84] including

$$F_a(r) = \frac{\alpha_a r}{1 + \beta_a r^2}, \tag{2.3}$$

$$F_p(r) = \frac{\alpha_p r^2}{1 + \beta_p r^2}, \tag{2.4}$$

where, r and $F_a(r)$: input/output amplitudes, $F_p(r)$: phase shift, α_a: linear gain.

2.3.2 Rapp model

In 1991, Rapp proposed an envelope model for SSPA as [82]

$$F_a(r) = \frac{gr}{\left[1 + \left(\frac{gr}{A_{os}}\right)^{2s}\right]^{1/2s}}, \tag{2.5}$$

where, r and $F_a(r)$: input/output amplitudes, g: small-signal gain, A_{os}: output
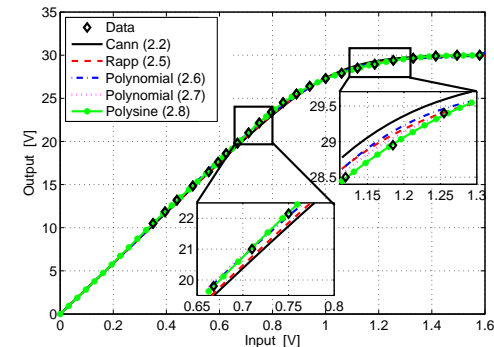

Figure 2.1: AM-AM functions of the Cann, Rapp, polynomial, odd-order polynomial and polysine models fitted to the measured data.

saturation level, and s: sharpness. Though absence of modulus operator (|.|) in the denominator, this model still incurs the problem as of (2.1).

2.3.3 Cann envelope model

Although originally developed as an instantaneous model, (2.2) can be used equally as an envelope model, suitable for AM-AM characteristics of most SSPAs [31]. The approximations of Cann new model (2.2) and Rapp model (2.5)

Table 2.1: Coefficients of the polynomial models (2.6), (2.7).

Model	a_1	a_2	a_3	a_4	a_5	a_6	a_7	a_8	a_9
(2.12)	30.02	-8.665	33.68	-40.19	12.39	0	0	0	0
(2.13)	28.60	0	8.310	0	-15.06	0	6.257	0	-0.872

to the real-world data are verified by curve fitting of these functions to the measured data from the L band Quasonix 10W amplifier [86]. Results are, for Rapp model: $g = 29.4$, $A_{os} = 30$ [V], $s = 4.15$, Squared Error Sum (SES) $\sigma_e^2 = 0.963$; new Cann model: $g = 29.4$, $A_{os} = 30$ [V], $s = 8.9$ and $\sigma_e^2 = 1.786$. For this particular HPA, Rapp model is little better fitted than Cann model. Figure 2.1 illustrates these fittings with the inclusion of other approximated curves discussed below.

2.3.4 Polynomial model

A complex polynomial power series of a finite order N is given by [31]:

$$y = F(x) = \sum_{n=1}^{N} a_n |x|^{n-1} x = \sum_{n=1}^{N} a_n \Psi_n^P[x], \qquad (2.6)$$

where, $\Psi_n^P[x] = |x|^{n-1}x$: basis functions, and a_n: complex coefficients.

Model (2.6) is not analytic at $r = |x| = 0$ by the existence of modulus operators $(|.|)$. However, if even order coefficients a_{2n} vanish, then for real-valued $x(t)$, (2.6) turns into the odd-order polynomial model of the form

$$y = \sum_{n=1}^{N} a_{2n-1} |x|^{2(n-1)} x = \sum_{n=1}^{N} a_{2n-1} x^{2n-1}. \qquad (2.7)$$

Model (2.7) is clearly analytic at $r = 0$ and is used as a counter example to model (2.6), showing that though having almost similar structure, they give quite different results. The above HPA measured data is then used to fit models (2.6) and (2.7), all with $N = 5$. Figure 2.1 depicts the approximated characteristics with their corresponding parameters shown in Table 2.1.

2.3.5 Proposed polysine model

While remaining to be analytic, the trigonometric functions are better fitted to data than the polynomial ones. Thus, we propose a nonlinear model as

$$y = \sum_{n=1}^{N} a_n \sin(b_n x), \qquad (2.8)$$

where, a_n and b_n are correspondingly amplitude and phase coefficients.

Chapter 4

Automatic Phase Estimation and Compensation for Nonlinear Distortions due to HPAs in MIMO-STBC Systems

4.1 Overview

Driven by the effectiveness of Sergienko's method for phase estimation in linear SISO M-QAM systems [78,79] and based on detailed analysis of the phase rotation effects for the nonlinear MIMO-STBC signals, this chapter presents a proposal of phase estimation and phase compensation for this nonlinear MIMO-STBC system. Different nonlinearities are included in the analyses and simulation to assess the effectiveness and reliability of the proposed schemes.

4.2 Phase rotation effect incurred by nonlinear HPAs for the MIMO-STBC signals

4.2.1 Nonlinear MIMO-STBC system model with phase estimation and compensation at the receiver

Figure 4.1 describes the proposed model, which is the supplementation of Figure 3.1 with phase estimation/compensation blocks succeeding SRRC receive filters. The signal processing at the transmitter has already been analysed
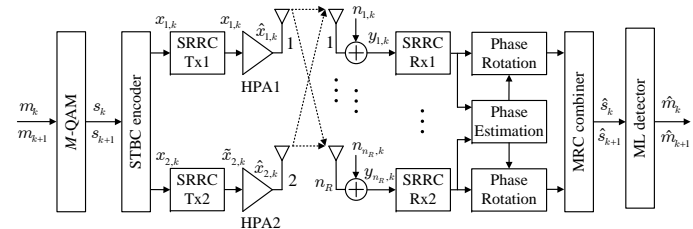

Figure 4.1: Proposed model with phase estimation and compensation.

in sub-section 3.2.1. However, since the most importance of the phase estimation proposal is the Gaussian approximation for the non-Gaussian model [67], then several typical HPA nonlinearities, including both AM-AM and especially, AM-PM characteristics investigated in Chapter 2 will be used to generate diversified nonlinearities for the system in consideration. The following HPAs

duced). Beyond this value, nonlinear distortions are too strong, and cannot be compensated even with the ideal predistortion scheme (inverse Saleh), so the quality of the system decreases very quickly.

3.4.2 Bit error ratio

The aggregate performance of the MIMO-STBC system with different pre-distorters is expressed in terms of bit error rate by E_b/N_0 as shown in Figure 3.6. At this *IBO* level, ideal Saleh predistortion is well approximated to the perfect linear system (dashed curve with legend "Linear").
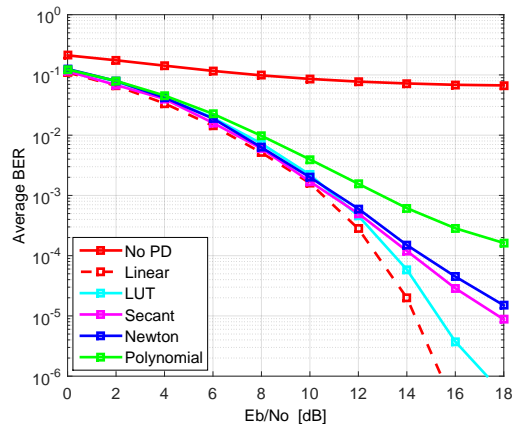

Figure 3.6: MISO-STBC system's BER(E_b/N_0) with different predistorters.

3.5 Summary of chapter 3

This chapter aims to fully investigate the effects of nonlinear distortions on MIMO-STBC system that have not been mentioned in previous publications. The analyses show that the transmit/receive filtering significantly increases the effects of nonlinear distortions in the system, the distribution of receive signals become non-Gaussian and so it is not easy to perform the analytical analysis. Thereby, limitations in the previous works are shown. Based on these analyses, four predistortion schemes are proposed to apply to the system. These diagrams are analyzed in detail and compared the performance through specific measures including EVM, MER and BER.

Table 2.2: Coefficients of the polysine model (2.8).

n	1	2	3	4	5
a_n	30.73	-0.6586	-0.1061	0.00955	0.1859
b_n	1.045	5.312	12.91	18.61	8.107

Table 2.3: Approximation performance of five models (SES σ_e^2).

Model	Cann (2.2)	Rapp (2.11)	Polynomial (2.12)	Polynomial (2.13)	Polysine (2.14)
SES	1.786	0.963	0.533	0.346	0.032

(2.8) is fixed to the above HPA data, resulting in parameters in Table 2.2. The fitting performances of these five models are measured using the SES listed in Table 2.3. Polysine model is almost one order of magnitude better in SES than the rest. The fitting performance of these models will reflect in the nonlinearity simulation results that are then discussed in section 2.4 bellow.

2.3.6 Other conventional HPA models

Beside the AM-AM, updated envelope models for SSPAs all consider the AM-PM conversion. However, all models discussed below are not analytic at $r = 0$ for most of the parameter sets and thus problem as of (2.5) still exists.

- *Modified Saleh model:* was proposed for LDMOS HPAs as [72]

$$F_a(r) = \frac{\alpha_a r}{\sqrt{1 + \beta_a r^3}}, \tag{2.9}$$

$$F_p(r) = \frac{\alpha_p}{\sqrt[3]{1 + r^4}} - \varepsilon_p, \tag{2.10}$$

where, $\alpha_a = 1.0536$, $\beta_a = 0.086$, $\alpha_p = 0.161$, and $\varepsilon_p = 0.124$ is a parameter set.

- *Modified Ghorbani model:* is suited for GaAs pHEMT HPAs [6] with

$$F_a(r) = \frac{\alpha_1 r^{\alpha_2} + \alpha_3 r^{\alpha_2+1}}{1 + \alpha_4 r^{\alpha_2}}, \tag{2.11}$$

$$F_p(r) = \frac{\beta_1 r^{\beta_2} + \beta_3 r^{\beta_2+1}}{1 + \beta_4 r^{\beta_2}}, \tag{2.12}$$

where, the model parameters are given by $\alpha_1 = 7.851$, $\alpha_2 = 1.5388$, $\alpha_3 = -0.4511$, $\alpha_4 = 6.3531$, $\beta_1 = 4.6388$, $\beta_2 = 2.0949$, $\beta_3 = -0.0325$, $\beta_4 = 10.8217$.

- *Modified Rapp model:* was introduced for GaAs pHEMT/CMOS HPAs at 60 GHz band with AM-AM function of (2.5) and AM-PM described as [21]

$$F_p(r) = \frac{\alpha r^{q_1}}{\left(1 + \left(\frac{r}{\beta}\right)^{q_2}\right)}, \tag{2.13}$$

where, $g = 16$, $A_{\mathrm{os}} = 1.9$, $s = 1.1$, $\alpha = -345$, $\beta = 0.17$, $q_1 = q_2 = 4$.

2.4 Applications in communication simulation

2.4.1 Simulation with two-tone testing signal

Two tones with $f_{1,2} = 7, 10$ [Hz] are used as inputs for 5 models. The IMP3/5 are shown in Figures 2.2(a), (b). New Cann, odd order polynomial and polysine models result in the required slope of 3 and 5 [dB/dB] as expected [37, 64]. However, full order polynomial, Rapp models fail in simulating the IMPs.
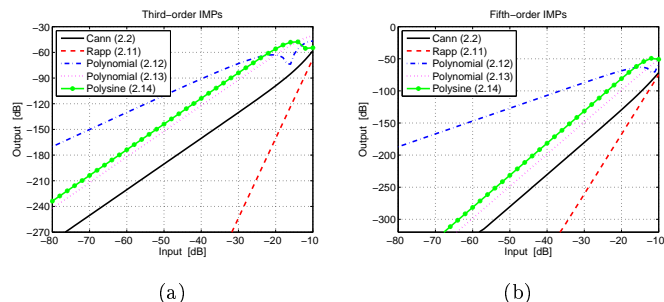

(a)   (b)

Figure 2.2: Third (a) and fifth (b) order IMPs of 5 models in Figure 2.1.

2.4.2 Simulation with continuous-spectrum testing signal

Consider the $1+7$ APSK as input with SRRC filter. Figure 2.3(a) illustrates Rx constellations by (2.2) and (2.7), manifesting relatively strong nonlinearity. Figure 2.3(b) depicts spectral regrowths of all 5 models. Then, either non-analyticity or larger approximation error could result in less accurate IMPs.
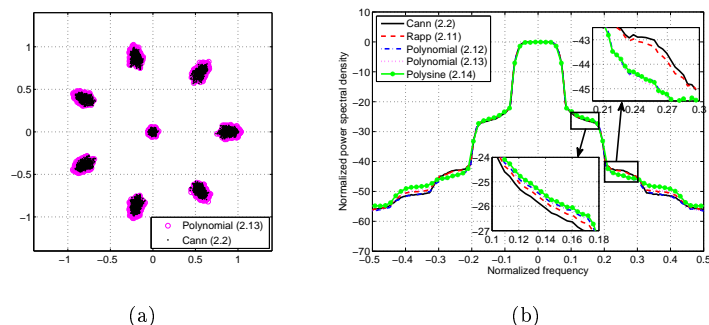

(a)   (b)

Figure 2.3: Results created from 1+7-APSK: a) constellations; b) spectra.

2.5 Summary of chapter 2

It is now clear that nonlinear HPA models satisfying analyticity and well-matching to measurements can ensure reliable simulation results.

3.4 Performance evaluation for predistorted MIMO-STBC systems

Basic parameters of predistortion algorithms: Ideal inverse Saleh using 10-bit LUT; adaptive secant method initialized by $PD_0 = 0$, $PD_1 = 1$, absolute recursive error $|PD_m - PD_{m+1}| < 10^{-6}$; adaptive Newton method initialized by $(P_a, P_p)_0 = (0,0)$, $(P_a, P_p)_1 = (1,1)$, absolute recursive error $|(P_a, P_p)_m - (P_a, P_p)_{m+1}| \leqslant 10^{-2}$; LMS polynomial approximation method using amplitude polynomial of order 5, phase polynomial of order 4, amplitude error $\varepsilon_a \leqslant 10^{-5}$, phase error $\varepsilon_p \leqslant 10^{-6}$, adaptive step sizes determined by their corresponding errors, $\mu_a(m) = |e_a(m)|/2$, $\mu_p(m) = |e_p(m)|/2$. All adaptive algorithms have same maximum iterations $N_{\mathrm{ite}} \leqslant 50$, avoiding the case of unsatisfying error conditions.
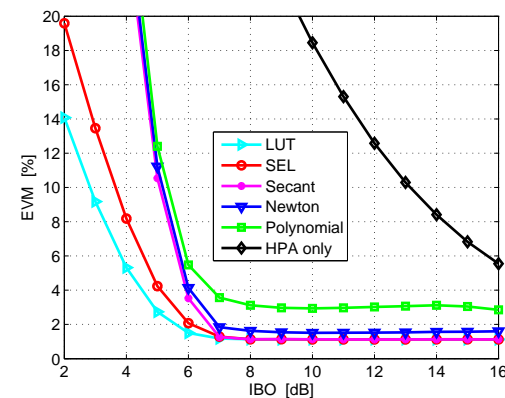

Figure 3.5: MIMO-STBC system's EVM(IBO) with different predistorters.

3.4.1 Error vector module

Figure 3.5 depicts EVMs versus IBO of systems: ideal inverse Saleh (LUT), soft envelope (SEL), adaptive secant method (Secant), adaptive Newton method (Newton), adaptive LMS polynomial approximation (Polynomial), and none predistortion (HPA only). The ability to improve the signal quality of the pre-distortion algorithms also decreases in this order. When using predistortion, at least the HPA operating point can reliably be pushed to a certain threshold of IBO (around $6 \sim 7$ dB, for the simulation parameter set and HPA model intro-

3.3.1 Ideal inverse Saleh predistortion

Predistortion functions (equations (28) and (30)) calculated by Chen in [87] are revised as

$$P_a(r) = \begin{cases} \dfrac{\alpha_a - \sqrt{\alpha_a^2 - 4\beta_a r^2}}{2\beta_a r}, & r \leqslant A_{\mathrm{os}}, \\[2mm] 1/\sqrt{\beta_a}, & r > A_{\mathrm{os}}, \end{cases} \qquad (3.8)$$

$$P_p(r) = \begin{cases} \dfrac{-\alpha_p\left(\alpha_a - \sqrt{\alpha_a^2 - 4\beta_a r^2}\right)^2}{\beta_p\left(\alpha_a - \sqrt{\alpha_a^2 - 4\beta_a r^2}\right)^2 + 4\beta_a^2 r^2}, & r \leqslant A_{\mathrm{os}}, \\[2mm] \dfrac{-\alpha_p}{\beta_a + \beta_p}, & r > A_{\mathrm{os}}. \end{cases} \qquad (3.9)$$

3.3.2 Adaptive secant predistortion

The concept of predistortion by secant method was proposed by Cavers J.K. [19] when he found an adaptive solution for PD by referring to the problem of solving algebraic equations. This is given by the recurrence relation [96,99]

$$PD_{m+1}(\tilde{x}) = \frac{PD_{m-1}(\tilde{x}) \cdot e(PD_m(\tilde{x})) - PD_m(\tilde{x}) \cdot e(PD_{m-1}(\tilde{x}))}{e(PD_m(\tilde{x})) - e(PD_{m-1}(\tilde{x}))}, \qquad (3.10)$$

starting with initial values $PD_0(\tilde{x}_k)$ and $PD_1(\tilde{x}_k)$.

3.3.3 Adaptive Newton predistortion

To reduce computational complexity, [102] proposed the root finding $PD_m(\tilde{x})$ in (3.10) by adaptive Newton method for the amplitude and phase predistortion functions, P_a^m and P_p^m where the true derivatives of Jacobian matrix are approximated by differential entropy:

$$\mathbf{J} = \begin{pmatrix} \dfrac{h_1(P_a^m, P_p^m) - h_1(P_a^{m-1}, P_p^m)}{P_a^m - P_a^{m-1}} & \dfrac{h_1(P_a^m, P_p^m) - h_1(P_a^m, P_p^{m-1})}{P_p^m - P_p^{m-1}} \\[3mm] \dfrac{h_2(P_a^m, P_p^m) - h_2(P_a^{m-1}, P_p^m)}{P_a^m - P_a^{m-1}} & \dfrac{h_2(P_a^m, P_p^m) - h_2(P_a^m, P_p^{m-1})}{P_p^m - P_p^{m-1}} \end{pmatrix}. \qquad (3.11)$$

3.3.4 Adaptive LMS polynomial-approximated predistortion

$P_a(r)$ and $P_p(r)$, could be approximated by the following polynomials [94]

$$P_a(r) = a_1 r + a_2 r^2 + a_3 r^3 + \ldots + a_l r^l = \mathbf{a}^T \mathbf{r}_a, \qquad (3.12)$$

$$P_p(r) = p_0 + p_1 r + p_2 r^2 + \ldots + a_m r^m = \mathbf{p}^T \mathbf{r}_p. \qquad (3.13)$$

The least mean square (LMS) algorithm [44] is then employed for calculating amplitude and phase coefficients $\mathbf{a}(m)$, $\mathbf{p}(m)$.

Chapter 3

Predistortion Methods for Nonlinear Distortions due to HPAs in MIMO-STBC Systems

3.1 Overview

Researches and developments of predistortion techniques for MIMO-STBC systems have been discussed in [73,74,81,94], however for simplification, all do not include transmit/receive filters in the system model, and thus only memoryless nonlinear effects are considered and resolved. Then, this chapter carries out a thorough analyses for the nonlinear MIMO-STBC with the filters introduced into the system model. Four predistortion schemes will be analyzed and applied to the system. Then, the performance of predistored system is measured by EVM, MER, and BER, showing their efficiency and effectiveness.

3.2 Nonlinear distortion effects in MIMO-STBC systems

3.2.1 MIMO-STBC $2 \times n_R$ system model

Signals output STBC encoder are of the form (1.6). Then, they are input to the SRRC shaping filters with continuous response

$$h(t) = \frac{1}{\sqrt{T}} \frac{\sin\left[\pi \frac{t}{T}(1-\alpha)\right] + 4\alpha \frac{t}{T}\cos\left[\pi \frac{t}{T}(1+\alpha)\right]}{\pi \frac{t}{T}\left[1 - \left(4\alpha \frac{t}{T}\right)^2\right]}. \qquad (3.1)$$

Its causal discrete-time response is given by

$$h[n] = \left. h(t) \right|_{t=n\frac{T}{M}}, \quad -\frac{N-1}{2} \leq n \leq \frac{N-1}{2}. \qquad (3.2)$$

At the k-th time slot, the output of the i-th filter, $i = 1, 2$, thus is of the form

$$\tilde{x}_{i,k} = x_{i,k} h[0] + \sum_{l \neq k, -\frac{N-1}{2} \leqslant l \leqslant \frac{N-1}{2}} x_{i,l} h[k-l] = x_{i,k} h[0] + n_{i,k}^{\mathrm{ISI}}. \qquad (3.3)$$

Therefore, signals input to the HPA also contain the ISI term $n_{i,k}^{\mathrm{ISI}}$, which then yields nonlinear ISI at the HPA output. For the purposed of comparison with previous publications, without considering the spectral regrowth effect as analysed in Chapter 2, here we use conventional HPA models including TWTA by Saleh model (2.3), (2.4) and SSPA by Rapp model (2.5).
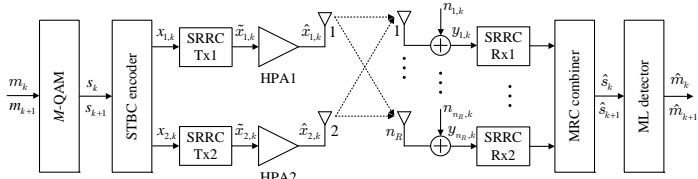
Figure 3.1: MIMO-STBC model with Tx-Rx filters and nonlinear HPAs.

3.2.2 Nonlinear distortion effects incurred by HPAs

Receive signals on the l-th branch, $1 \leqslant l \leqslant n_R$, in time slots k and $(k+1)$ are

$$y_{l,k} = h_{l,1}\hat{s}_k + h_{l,2}\hat{s}_{k+1} + n_{l,k}, \tag{3.4}$$

$$y_{l,k+1} = -h_{l,1}\hat{s}_{k+1}^* + h_{l,2}\hat{s}_k^* + n_{l,k+1}. \tag{3.5}$$

Applying maximum ratio combining [7], these receive signals are processed as

$$\bar{s}_{l,k} = h_{l,1}^* y_{l,k} + h_{l,2} y_{l,k+1}^*, \tag{3.6}$$

$$\bar{s}_{l,k+1} = h_{l,2}^* y_{l,k} - h_{l,1} y_{l,k+1}^*. \tag{3.7}$$

Using linearized model (1.3) for the HPA input/output signals s_k and $\hat{s}_k$, then
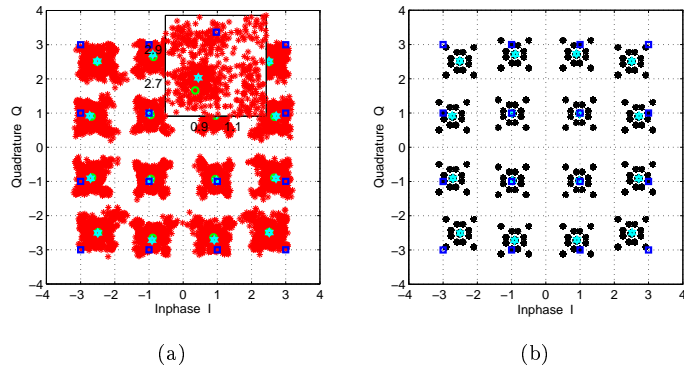

(a) (b)

Figure 3.2: Receive signals after MRC: a) with filters; b) without filters.

signals after MRC are affected by nonlinear noise, nonlinear ISI and nonlinear ICI. These effects are illustrated in Figure 3.2(a), simulated by: 16-QAM; filters' rolloff factor $\alpha = 0.2$, input/output sampling rates $F_d = 1$, $F_s = 16F_d$, group delay $Dl = 10$; HPA Saleh model $\alpha_a = 2$, $\beta_a = 1$, $\alpha_p = \pi/3$, $\beta_p = 1$, $IBO = 10$ dB.

Figure 3.2(b) is yielded from the same model but without filtering. Thus, such models, also as in [73,74,81,94], do not fully represent HPA's nonlinear

effects and give (much) more optimistic results. Further, the change of receive signal statistics, that actually reflect the nonlinear ISI and ICI effects, is not observed in Figure 3.2(b), making deceptive assumption for analytical analyses.
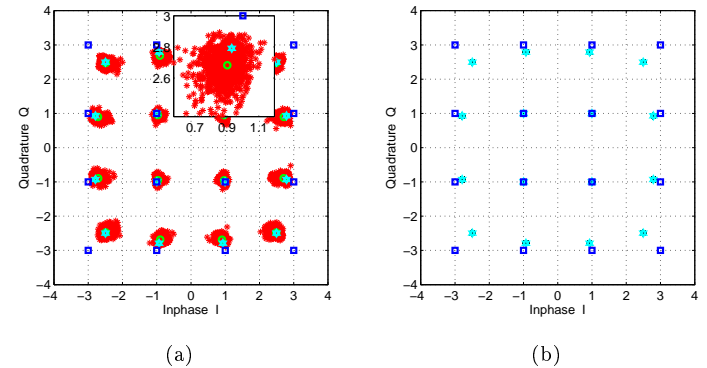

(a) (b)

Figure 3.3: For HPA model utilized in [81]: a) with filters; b) without filters.

Moreover, by Figure 3.2(b), even without filtering ICI still exists under nonlinear HPA effects. Therefore, using orthogonality of STBC code to decompose the MIMO system into SISO equivalent ones as equation (8) in [81] is an over simplification, only reasonable when the nonlinearity is weak, and without AM-PM distortion. Then, the ICI will be negligible, the cluster points shrink into a single point with only amplitude compression effect exists. This fact is demonstrated by Figure 3.3(b) with the HPA parameters used in [81]. Moreover, if the system model having Tx-Rx filters as it practically is, the signal quality is also significantly degraded as illustrated in Figure 3.3(a). Obviously, the receive signals are non-Gaussian, making analytical analyses impossible.

3.3 Predistortion schemes
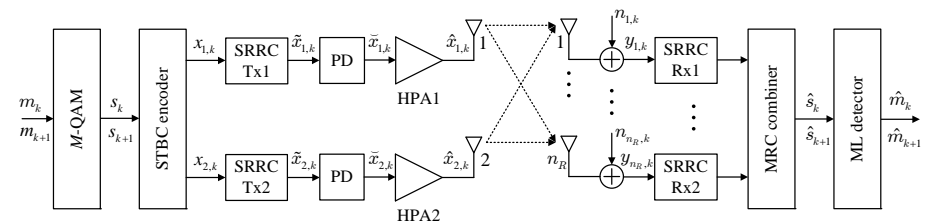
The proposed system model is illustrated in Figure 3.4.

Figure 3.4: MIMO-STBC system model with predistorters.